**Opposing Activities Protect Against Age-Onset Proteotoxicity**
Ehud Cohen, *et al.*
*Science* **313**, 1604 (2006);
DOI: 10.1126/science.1124646

39. C. P. Joshi *et al.*, *New Phytol.* **164**, 53 (2004).
40. A. Samuga, C. P. Joshi, *Gene* **334**, 73 (2004).
41. F. Roudier *et al.*, *Plant Cell* **17**, 1749 (2005).
42. R. M. Perrin *et al.*, *Science* **284**, 1976 (1999).
43. R. W. Whetten, J. J. Mackay, R. R. Sederoff, *Annu. Rev. Plant Physiol. Plant Mol. Biol.* **49**, 585 (1998).
44. J. Ehlting *et al.*, *Plant J.* **42**, 618 (2005).
45. J. Raes, A. Rohde, J. H. Christensen, Y. Van de Peer, W. Boerjan, *Plant Physiol.* **133**, 1051 (2003).
46. D. M. O'Malley, S. Porter, R. R. Sederoff, *Plant Physiol.* **98**, 1364 (1992).
47. J. J. Mackay, W. W. Liu, R. Whetten, R. R. Sederoff, D. M. Omalley, *Mol. Gen. Genet.* **247**, 537 (1995).
48. J. Schrader *et al.*, *Plant Cell* **16**, 2278 (2004).
49. S. Whitham, S. McCormick, B. Baker, *Proc. Natl. Acad. Sci. U.S.A.* **93**, 8776 (1996).
50. G. M. Gebre, T. J. Tschaplinski, G. A. Tuskan, D. E. Todd, *Tree Physiol.* **18**, 645 (1998).
51. G. Arimura, D. P. W. Huber, J. Bohlmann, *Plant J.* **37**, 603 (2004).
52. D. J. Peters, C. P. Constabel, *Plant J.* **32**, 701 (2002).
53. C.-J. Tsai, S. A. Harding, T. J. Tschaplinski, R. L. Lindroth, Y. Yuan, *New Phytol.* **172**, 47 (2006).
54. M. M. De Sá, R. Subramaniam, F. E. Williams, C. J. Douglas, *Plant Physiol.* **98**, 728 (1992).
55. R. L. Lindroth, S. Y. Hwang, *Biochem. Syst. Ecol.* **24**, 357 (1996).
56. B. Winkel-Shirley, *Curr. Opin. Plant Biol.* **5**, 218 (2002).
57. G. J. Tanner *et al.*, *J. Biol. Chem.* **278**, 31647 (2003).
58. S. Aubourg, A. Lecharny, J. Bohlmann, *Mol. Genet. Genomics* **267**, 730 (2002).
59. M. A. Costa *et al.*, *Phytochemistry* **64**, 1097 (2003).
60. D. Cukovic, J. Ehlting, J. A. VanZiffle, C. J. Douglas, *Biol. Chem.* **382**, 645 (2001).
61. J. M. Shockey, M. S. Fulda, J. Browse, *Plant Physiol.* **132**, 1065 (2003).
62. I. E. Somssich, P. Wernert, S. Kiedrowski, K. Hahlbrock, *Proc. Natl. Acad. Sci. U.S.A.* **93**, 14199 (1996).
63. L. Li *et al.*, *Plant Cell* **13**, 1567 (2001).
64. B. C. Meyers, S. Kaushik, R. S. Nandety, *Curr. Opin. Plant Biol.* **8**, 129 (2005).
65. L. Deslandes *et al.*, *Proc. Natl. Acad. Sci. U.S.A.* **99**, 2404 (2002).
66. E. J. Mellerowicz, M. Baucher, B. Sundberg, W. Boerjan, *Plant Mol. Biol.* **47**, 239 (2001).
67. A. P. Mähönen *et al.*, *Science* **311**, 94 (2006).
68. S. Andersson-Gunneras *et al.*, *Plant J.* **34**, 339 (2003).
69. J. M. Hellgren, K. Olofsson, B. Sundberg, *Plant Physiol.* **135**, 212 (2004).
70. M. G. Cline, K. Dong-Il, *Ann. Bot. (London)* **90**, 417 (2002).
71. R. Ruonala, P. Rinne, M. Baghour, H. Tuominen, J. Kangasjärvi, *Plant J.*, in press.
72. R. Moyle *et al.*, *Plant J.* **31**, 675 (2002).
73. D. Weijers *et al.*, *EMBO J.* **24**, 1874 (2005).
74. G. Hagen, T. Guilfoyle, *Plant Mol. Biol.* **49**, 373 (2002).
75. M. E. Eriksson, M. Israelsson, O. Olsson, T. Moritz, *Nat. Biotechnol.* **18**, 784 (2000).
76. T. Kakimoto, *Science* **274**, 982 (1996).
77. T. Kiba, K. Aoki, H. Sakakibara, T. Mizuno, *Plant Cell Physiol.* **45**, 1063 (2004).
78. T. Nakano, K. Suzuki, T. Fujimura, H. Shinshi, *Plant Physiol.* **140**, 411 (2006).
79. F. Sterky *et al.*, *Proc. Natl. Acad. Sci. U.S.A.* **101**, 13951 (2004).
80. J. Ehlting *et al.*, *Plant J.* **42**, 618 (2005).
81. B. C. Meyers, S. Kaushik, R. S. Nandety, *Curr. Opin. Plant Biol.* **8**, 129 (2005).
82. M. W. Jones-Rhoades, D. P. Bartel, *Mol. Cell* **14**, 787 (2004).


83. We thank the U.S. Department of Energy, Office of Science for supporting the sequencing and assembly portion of this study; Genome Canada and the Province of British Columbia for providing support for the BAC end, BAC genotyping, and full-length cDNA portions of this study; the Umeå University and the Royal Technological Institute (KTH) in Stockholm for supporting the EST assembly and annotation portion of this study; the membership of the International *Populus* Genome Consortium for supplying genetic and genomics resources used in the assembly and annotation of the genome; the NSF Plant Genome Program for supporting the development of Web-based tools; T. H. D. Bradshaw and R. Stettler for input and reviews on draft copies of the manuscript; J. M. Tuskan for guidance and input during the analysis and writing of the manuscript; and the anonymous reviewers who provided critical input and recommendations on the manuscript. GenBank Accession Number: AARH00000000.


**Supporting Online Material**

www.sciencemag.org/cgi/content/full/313/5793/1596/DC1
Materials and Methods
Figs. S1 to S15
Tables S1 to S14
References

13 April 2006; accepted 9 August 2006
10.1126/science.1128691

# Opposing Activities Protect Against Age-Onset Proteotoxicity

**Ehud Cohen,[1]* Jan Bieschke,[2]* Rhonda M. Perciavalle,[1] Jeffery W. Kelly,[2] Andrew Dillin[1]†**

**Aberrant protein aggregation is a common feature of late-onset neurodegenerative diseases, including Alzheimer's disease, which is associated with the misassembly of the $A\beta_{1-42}$ peptide. Aggregation-mediated $A\beta_{1-42}$ toxicity was reduced in *Caenorhabiditis elegans* when aging was slowed by decreased insulin/insulin growth factor–1–like signaling (IIS). The downstream transcription factors, heat shock factor 1, and DAF-16 regulate opposing disaggregation and aggregation activities to promote cellular survival in response to constitutive toxic protein aggregation. Because the IIS pathway is central to the regulation of longevity and youthfulness in worms, flies, and mammals, these results suggest a mechanistic link between the aging process and aggregation-mediated proteotoxicity.**

Late-onset human neurodegenerative diseases including Alzheimer's (AD), Huntington's, and Parkinson's diseases are genetically and pathologically linked to aberrant protein aggregation (*1*, *2*). In AD, formation of aggregation-prone peptides, particularly $A\beta_{1-42}$, by endoproteolysis of the amyloid precursor protein (APP) is associated with the disease through an unknown mechanism (*3*, *4*). Whether intracellular accumulation or extracellular deposition of $A\beta_{1-42}$ initiates the pathological process is a key unanswered question (*5*). Typically, individuals who carry AD-linked mutations present with clinical symptoms during their fifth or sixth decade, whereas sporadic cases appear after the seventh decade. Why aggregation-mediated toxicity emerges late in life and whether it is mechanistically linked to the aging process remain unclear.

Perhaps the most prominent pathway that regulates life span and youthfulness in worms, flies, and mammals is the insulin/insulin growth factor (IGF)–1–like signaling (IIS) pathway (*6*). In the nematode *Caenorhabditis elegans*, the sole insulin/IGF-1 receptor, DAF-2 (*7*), initiates the transduction of a signal that causes the phosphorylation of the FOXO transcription factor, DAF-16 (*8*, *9*), preventing its translocation to the nucleus (*10*). This negative regulation of DAF-16 compromises expression of its target genes, decreases stress resistance, and shortens the worm's life span. Thus, inhibition of *daf-2* expression creates long-lived, youthful, stress-resistant worms (*11*). Similarly, suppression of the mouse DAF-2 ortholog, IGF1-R, creates long-lived mice (*12*). Recent studies indicate that, in worms, life-span extension due to reduced *daf-2* activity is also dependent upon heat shock factor 1 (HSF-1). Moreover, increased expression of *hsf-1* extends worm life span in a *daf-16*–dependent manner (*13*). That the DAF-16 and HSF-1 transcriptomes result in the expression of numerous chaperones (*13*, *14*) suggests that the integrity of protein folding could play a key role in life-span determination and the amelioration of aggregation-associated proteotoxicity. Indeed, amelioration of Huntington-associated proteotoxicity by slowing the aging process in worms has been reported (*13*, *15*, *16*).

**Reduced IIS activity lowers $A\beta_{1-42}$ toxicity.** One hypothesis to explain late-onset aggregation-associated toxicity posits that the deposition of toxic aggregates is a stochastic process, governed by a nucleated polymerization and requiring many years to initiate disease. Alternatively, aging could enable constitutive aggregation to become toxic as a result of declining detoxification activities. To distinguish between these two possibilities, we asked what role the aging process plays in $A\beta_{1-42}$ aggregation-mediated toxicity in a *C. elegans* model featuring intracellular $A\beta_{1-42}$ expression (*17*). If $A\beta_{1-42}$ toxicity results from a non-age-related nucleated polymerization, animals that express $A\beta_{1-42}$ and whose life span has been extended would be expected to succumb to $A\beta_{1-42}$ toxicity at the same rate as those with a natural life span. However, if the aging process plays a role in detoxifying an ongoing protein aggregation process, alteration of the aging program

[1]Molecular and Cell Biology Laboratory, Salk Institute for Biological Studies, 10010 North Torrey Pines Road, La Jolla, CA 92037, USA. [2]Department of Chemistry and Skaggs Institute of Chemical Biology, Scripps Research Institute, 10550 North Torrey Pines Road, La Jolla, CA 92037, USA.

*These authors contributed equally to this work.
†To whom correspondence should be addressed E-mail: dillin@salk.edu

would postpone the initiation of aggregation-mediated toxicity. To examine these hypotheses, we used worms that express the human $A\beta_{1-42}$ minigene driven by the *unc-54* promoter (strain CL2006), referred hereafter as $A\beta_{1-42}$ worms (*18*). Accordingly, $A\beta_{1-42}$ is solely expressed within the body wall muscles, resulting in their paralysis (*18*). The unaffected neighboring muscles serve as an intraorganismal control in the RNA interference (RNAi)–based experiments that alter aging (movie S1).

We first tested whether *daf-2* RNAi extends the life span of $A\beta_{1-42}$ worms. $A\beta_{1-42}$ animals grown on potent *daf-2* RNAi bacteria (*19*) exhibited increased life spans compared with control $A\beta_{1-42}$ worms grown on empty RNAi vector (EV) bacteria (Fig. 1A), similar to previous results with wild-type *C. elegans* (*11*). *daf-2* RNAi treatment also decreased the fraction of paralyzed worms compared with control animals over a 12-day time course (Fig. 1B and movies S1 and S2). At day 10 of adulthood, 50% of the control worms were paralyzed compared with 10% of the *daf-2* RNAi worms. *C. elegans* not expressing $A\beta_{1-42}$ showed no aging-related paralysis through 9 days and less than 7% showed paralysis after 12 days (fig. S1). Collectively, these data demonstrate that alteration of the aging program suppresses the pathological effect of $A\beta_{1-42}$ expression within the body wall muscles of *C. elegans*. Thus, $A\beta_{1-42}$ proteotoxicity does not appear to be a stochastic process, but it is highly dependent on the aging process.

***Daf-16* and *Hsf-1* are required for the protective effect of reduced IIS.** To understand the mechanism by which reduced IIS protected against $A\beta_{1-42}$ proteotoxicity, we asked whether *daf-16* and/or *hsf-1*, genes that encode transcription factors necessary, but not sufficient, for the full extended life span of *daf-2* mutant animals (*10*, *13*), were also required for amelioration of proteotoxicity by *daf-2* RNAi. Dilution of *daf-2* RNAi bacteria with equal amounts of either effective *hsf-1* (fig. S2) or *daf-16* (*19*) RNAi bacteria abolished the *daf-2* RNAi protective effect (Fig. 1C). A correspondingly equal dilution of *daf-2*, *daf-16*, or *hsf-1* with the EV bacteria did not influence the paralysis phenotype of each RNAi treatment (fig. S3). Therefore, analogous to the roles of *daf-16* and *hsf-1* in the regulation of aging by *daf-2*, both *daf-16* and *hsf-1* are necessary for the reduced IIS-mediated amelioration of $A\beta_{1-42}$ proteotoxicity in the *C. elegans* body wall muscles.

We also tested whether reduction of *daf-16* or *hsf-1* affected paralysis rates in animals with an intact *daf-2*. To avoid potential developmental disorders due to RNAi knockdown, we individually inactivated *daf-2*, *daf-16*, or *hsf-1* only during adulthood, the period required for the IIS pathway to regulate the aging process (*19*). As before, *daf-2* RNAi reduced the number of paralyzed worms (Fig. 1D). In contrast, either *daf-16* or *hsf-1* RNAi increased the number of paralyzed animals after 8 days. Reduction of *hsf-1* during development and adulthood increased the rate of paralysis relative to *hsf-1* reduction during adulthood only (Fig. 1E). In contrast, rates of paralysis of animals grown on *daf-16* RNAi bacteria during development and adulthood versus adulthood only were very similar.

We evaluated the possibility that RNAi utilization caused differential expression of $A\beta_{1-42}$. Quantitative reverse transcription polymerase chain reaction (RT-PCR) experiments indicated that the amounts of $A\beta_{1-42}$ messenger RNA (mRNA) transcripts within $A\beta_{1-42}$ worms grown on EV, *daf-2*, *daf-16*, or *hsf-1* RNAi bacteria were nearly identical (fig. S4A). In addition, Western blot (WB) analysis revealed that soluble $A\beta_{1-42}$ amounts were equivalent in all RNAi applications (fig. S4B). Thus, the different degrees of proteotoxicity cannot be explained by modulation of $A\beta_{1-42}$ expression.

Taken together, these results suggest that DAF-16 and HSF-1 target genes are jointly essential for the $A\beta_{1-42}$ detoxification mediated

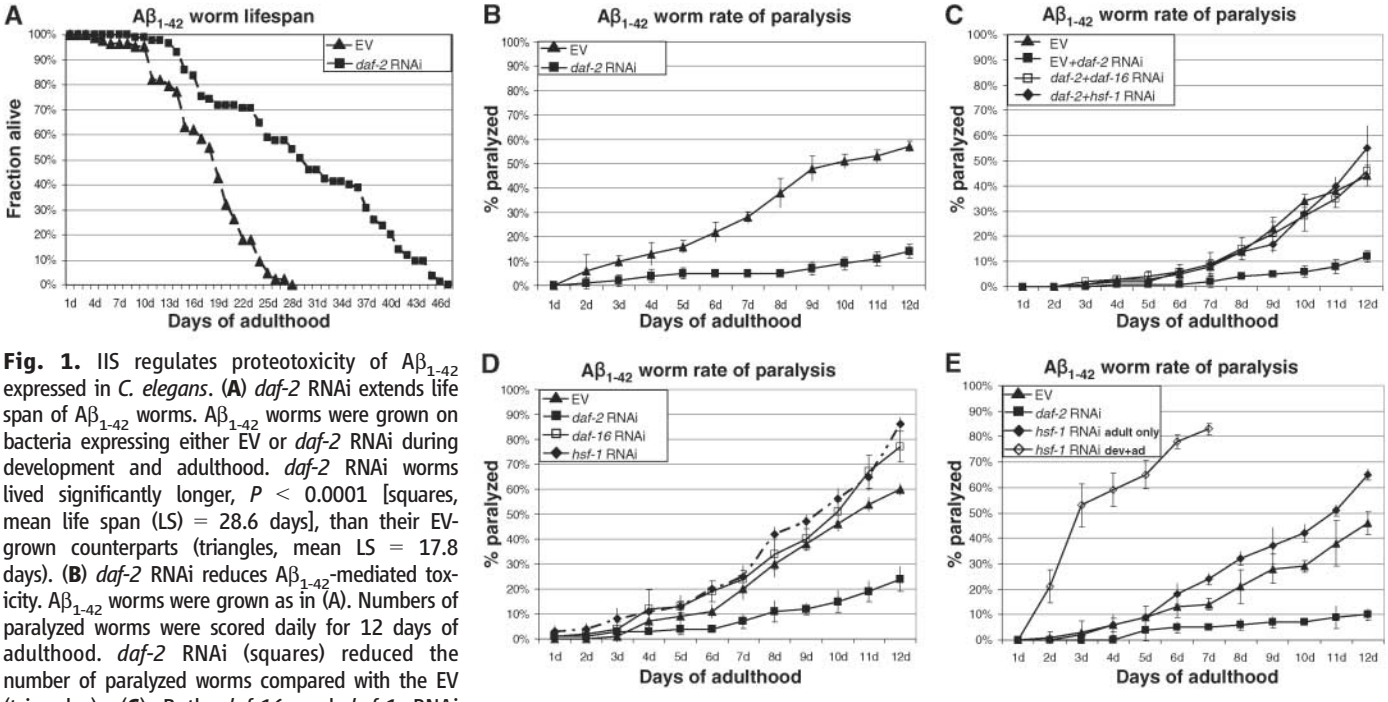


**Fig. 1.** IIS regulates proteotoxicity of $A\beta_{1-42}$ expressed in *C. elegans*. (**A**) *daf-2* RNAi extends life span of $A\beta_{1-42}$ worms. $A\beta_{1-42}$ worms were grown on bacteria expressing either EV or *daf-2* RNAi during development and adulthood. *daf-2* RNAi worms lived significantly longer, $P < 0.0001$ [squares, mean life span (LS) = 28.6 days], than their EV-grown counterparts (triangles, mean LS = 17.8 days). (**B**) *daf-2* RNAi reduces $A\beta_{1-42}$-mediated toxicity. $A\beta_{1-42}$ worms were grown as in (A). Numbers of paralyzed worms were scored daily for 12 days of adulthood. *daf-2* RNAi (squares) reduced the number of paralyzed worms compared with the EV (triangles). (**C**) Both *daf-16* and *hsf-1* RNAi abolished the protective effect of *daf-2* RNAi toward $A\beta_{1-42}$ toxicity. $A\beta_{1-42}$ worms were grown during development and adulthood on EV bacteria (triangles) or on dilutions of equal amounts of bacteria expressing the following RNAi species: *daf-2* and EV (solid squares), *daf-2* and *daf-16* (open squares), or *daf-2* and *hsf-1* (diamonds). (**D**) *daf-16* or *hsf-1*RNAi during adulthood results in an elevated rate of paralysis late in life. $A\beta_{1-42}$ worms were developed on EV and were transferred at day 1 of adulthood to bacteria expressing either EV (triangles), *daf-2* RNAi (solid squares), *daf-16* RNAi (open squares), or *hsf-1* RNAi (diamonds). *daf-2* RNAi reduced the number of paralyzed animals, whereas both *daf-16* and *hsf-1* RNAi increased the number of paralyzed worms late in life compared with the EV. (**E**) Reduced expression of *hsf-1* during development (dev) and adulthood (ad) further accelerates the rate of paralysis. $A\beta_{1-42}$ worms were grown during development and adulthood on bacteria expressing either EV (triangles), *daf-2* RNAi (squares) or *hsf-1* RNAi (open diamonds) or were developed on EV and transferred to *hsf-1* RNAi bacteria on day 1 of adulthood (solid diamonds). Error bars indicate standard deviations.

by inhibition of the IIS pathway. However, the HSF-1 transcriptome appears to play a more important role in suppressing $A\beta_{1-42}$-mediated toxicity, especially during development (Fig. 1E).

**High molecular weight $A\beta_{1-42}$ aggregates do not correlate with toxicity.** How could DAF-16 and HSF-1 transcriptomes protect worms from proteotoxicity? One possibility is that these transcriptomes prevent the formation of high molecular weight (high-MW) aggregates that are linked to toxicity. Alternatively, these transcriptomes could detoxify smaller oligomers that appear to mediate toxicity (*4*, *20*). To evaluate these possibilities, we asked whether *daf-2* RNAi mediated protection from $A\beta_{1-42}$ proteotoxicity and suppression of this protective effect by knockdown of either *daf-16* or *hsf-1* expression correlated with the amount of high-MW $A\beta_{1-42}$ aggregates. $A\beta_{1-42}$ worms were grown to day 1 of adulthood on EV or on *daf-2*, *daf-16*, or *hsf-1* RNAi bacteria. The worms were homogenized and centrifuged for 3 min at 3000 revolutions per min (rpm) to afford pellet and post debris supernatant (PDS) fractions (fig. S5A) that were evaluated separately (fig. S5, B and C). The PDS was subjected to ultracentrifugation, revealing the presence of high-MW $A\beta_{1-42}$ aggregates (Fig. 2A). If high-MW $A\beta_{1-42}$ aggregates were the toxic species, then *daf-2* RNAi animals would be expected to have less high-MW aggregates, and *daf-16* and *hsf-1* RNAi animals would be expected to accumulate more. PDS from *hsf-1* RNAi worms have the most high-MW aggregates, followed by *daf-2* and EV RNAi, whereas in *daf-16* RNAi worms the aggregates are hardly detectable. This observation is not consistent with high-MW $A\beta_{1-42}$ aggregates being the toxic species.

$A\beta_{1-42}$ aggregates in the PDS fraction were quantified with an in vitro kinetic aggregation assay, which is at least three orders of magnitude more sensitive than WB analysis (fig. S6). This assay enables the detection of small amounts of aggregates that can seed an $A\beta_{1-40}$ nucleated polymerization reaction in vitro. $A\beta_{1-42}$ worm PDS was sonicated to generate small fibrils (fig. S7). Addition of sonicated PDS to an in vitro $A\beta_{1-40}$ fibril formation assay would be expected to shorten the lag phase associated with the initiation of $A\beta_{1-40}$ aggregation in a fashion that is dependent on the concentration of fibrillar seeds (*21*). PDS from $A\beta_{1-42}$ worms grown to day 1 of adulthood on EV, *daf-2*, *daf-16*, or *hsf-1* RNAi bacteria were evaluated in vitro by assessing the time for half maximal aggregation of $A\beta_{1-40}$ ($t_{50}$) (Fig. 2B). Reactions seeded with PDS of *hsf-1* RNAi worms had significantly ($P < 0.0002$) faster $A\beta_{1-40}$ aggregation than did the control worms (EV). Similarly, homogenates from *daf-2* RNAi worms accelerated aggregation compared with the control worms ($P < 0.02$), but less than PDS from *hsf-1* RNAi worms. Lastly, *daf-16* RNAi worms harbored the least seeding competent aggregates. An in vitro kinetic aggregation assay using *hsf-1* RNAi worms not expressing $A\beta_{1-42}$ confirmed that the lag phase shortening is completely dependent on the presence of $A\beta_{1-42}$ (fig. S8).

Within the worm debris, less high-MW aggregates were found in the EV and *daf-2* RNAi-treated $A\beta_{1-42}$ worms compared with the increased amount found when *hsf-1* was reduced (Fig. 2, C and D). In contrast to *hsf-1* RNAi treatment, the least amount of high-MW $A\beta_{1-42}$ aggregates was found in the debris of *daf-16* RNAi worms. Strictly analogous results were observed by growing the $A\beta_{1-42}$ worms to day 3 of adulthood (Fig. 2E). Formic acid extraction of all of the $A\beta_{1-42}$ worm debris before analysis also indicated that *hsf-1* RNAi worms contained more high-MW $A\beta_{1-42}$ than did *daf-16* RNAi worms.

The relative amounts of $A\beta_{1-42}$ aggregates observed in the PDS and in the worm debris analyzed by WB rank order identically, with *hsf-1* RNAi worms having the most, followed by *daf-2* RNAi worms, then the $A\beta_{1-42}$ worms grown on EV bacteria, and lastly *daf-16* RNAi worms.

By using multiple ultracentrifugation steps with a final analysis by atomic force microscopy (AFM), we directly visualized high-density material purified from $A\beta_{1-42}$ worm PDS. Fibrillar structures were detected only in the *hsf-1* RNAi worms but not in PDS fractions of EV control (fig. S9), *daf-2*, or *daf-16* RNAi worms. To verify that the fibrillar structures observed by AFM contain $A\beta_{1-42}$, we used immunoelectron microscopy (immuno-EM) (fig. S10A). Quantification and distribution analysis of the gold particles labeling Aβ indicated that *hsf-1* RNAi treatment results in the most intense and specific signal. The PDS of $A\beta_{1-42}$ worms fed EV or *daf-2* RNAi bacteria had a weaker signal, whereas the *daf-16* RNAi worms had the least intense signal (Fig. 2F). Wild-type worms not expressing $A\beta_{1-42}$ that were fed *hsf-1* RNAi bacteria (negative control, fig. S10B) and in vitro aggregated $A\beta_{1-40}$ (positive control, fig. S10C) confirmed the immunogold particle signal specificity. Lastly, $A\beta_{1-42}$ worms were grown to day 2 of adulthood on the various RNAi species, and Aβ was visualized within the intact worm by using immunofluorescence (IF) microscopy. *daf-2* RNAi and EV worms had similar intermediate intensities, *hsf-1* RNAi-treated $A\beta_{1-42}$ worms exhibited the most intense signal, and *daf-16* RNAi treatment resulted in the weakest signal (Fig. 2G).

Collectively, results from five independent methods studying worm debris, PDS, and intact worms all indicate that *hsf-1* RNAi worms contain the largest amount of fibrils and high-MW $A\beta_{1-42}$ aggregates and that *daf-2* RNAi worms contain slightly more fibrils than their EV-treated counterparts, whereas *daf-16* RNAi worms contain the fewest fibrils and high-MW $A\beta_{1-42}$ aggregates. This points to a lack of correlation between high-MW $A\beta_{1-42}$ aggregates and $A\beta_{1-42}$-mediated toxicity, because (i) *daf-2* RNAi reduces toxicity but slightly enhances the amount of high-MW aggregates, (ii) *daf-16* RNAi increases toxicity but reduces the amount of high-MW aggregates, and (iii) *hsf-1* RNAi increases both toxicity and amount of high-MW $A\beta_{1-42}$ aggregates. The detection of aggregated $A\beta_{1-42}$ in early adulthood (days 1 to 2 of adulthood), before onset of paralysis (days 5 to 12), suggests that protein aggregation occurs early and throughout the life of the worm and is counteracted by aging-related processes to reduce toxicity.

**HSF-1 but not DAF-16 controls disaggregation of $A\beta_{1-42}$ aggregates.** Our findings suggest that two opposing mechanisms, regulated by the IIS pathway, protect worms from $A\beta_{1-42}$ mediated toxicity: The HSF-1 transcriptome regulates disaggregation, whereas the DAF-16 transcriptome mediates the formation of less-toxic high-MW aggregates. The latter is analogous to the aggregation-mediated neuroprotection invoked in Huntington's disease (*22*, *23*). Both activities appear to be required to protect the $A\beta_{1-42}$ worms from early-onset paralysis associated with proteotoxicity. Inhibiting the HSF-1 transcriptome during worm development is more deleterious than DAF-16 inhibition toward $A\beta_{1-42}$ toxicity, suggesting the former is the more important pathway (Fig. 1E). Thus, it is plausible that the HSF-1–controlled disaggregation and degradation pathway is the preferred pathway, whereas the DAF-16–controlled active aggregation is the backup pathway used mainly under severe stress conditions. We suppose that the HSF-1–controlled disaggregation pathway in the $A\beta_{1-42}$ worms is constantly overloaded. Thus, the DAF-16–regulated active aggregation machinery is continually assisting. Accordingly, *daf-2* RNAi worms have slightly more high-MW aggregates than EV animals because both the HSF-1–regulated and the DAF-16–regulated pathways are fully active.

To test the hypothesis that $A\beta_{1-42}$ disaggregation in the worm is regulated by HSF-1 but not DAF-16, we developed an in vitro assay to measure disaggregation of $A\beta_{1-40}$ fibrils by worm PDS. Time-dependent disaggregation of $A\beta_{1-40}$ fibrils in vitro, in the presence and absence of worm PDS, was quantified. To exclude the possibility of monitoring proteasomal and/or proteolytic degradation rather than disaggregation, we performed experiments in the presence of either (i) the proteasome inhibitor epoxomicin (10 μM) (fig. S11) or (ii) protease inhibitor cocktail. In buffer alone (Fig. 3A) and with added bovine serum albumin (BSA) (0.5 mg/ml), the fibrils were stable for at least 36 hours. In contrast, $A\beta_{1-40}$ fibrils underwent disaggregation when treated with PDS from $A\beta_{1-42}$ worms. Heat inactivation of PDS (95°C for 10 min) destroyed the disaggregation activity (Fig. 3A). The amount of $A\beta_{1-40}$ detected by WB after 17 and 96 hours of incubation with PDS in the absence of protease inhibitors was reduced, indicating that $A\beta_{1-40}$ was proteolyzed subsequent to disaggregation (Fig. 3B). In contrast, heat-inactivated PDS had

no detectable effect on the amount of $A\beta_{1-40}$. In the presence of a cocktail of protease inhibitors, $A\beta_{1-40}$ fibrils were disassembled but not degraded (Fig. 3C). Proteasome inhibitor alone did not prevent proteolysis, although more detailed experiments are needed before excluding proteasome involvement. $A\beta_{1-40}$ fibrils prepared in vitro were visible by AFM before treatment with worm PDS and after a 36-hour incubation with buffer, but not after incubation with PDS of EV-treated $A\beta_{1-42}$ worms (Fig. 3D). Collectively, the results confirm that the assay detects disaggregation activity of worm homogenates and demonstrate that worm PDS also proteolyses $A\beta_{1-40}$; yet, we can dissociate these activities with the appropriate use of protease inhibitors. In the presence of protease inhibitors, $A\beta_{1-40}$ fibrils will spontaneously reform if a longer time window (20 to 40 hours) is observed.

Does the disaggregation activity found within worm PDS reduce the toxicity of $A\beta_{1-40}$

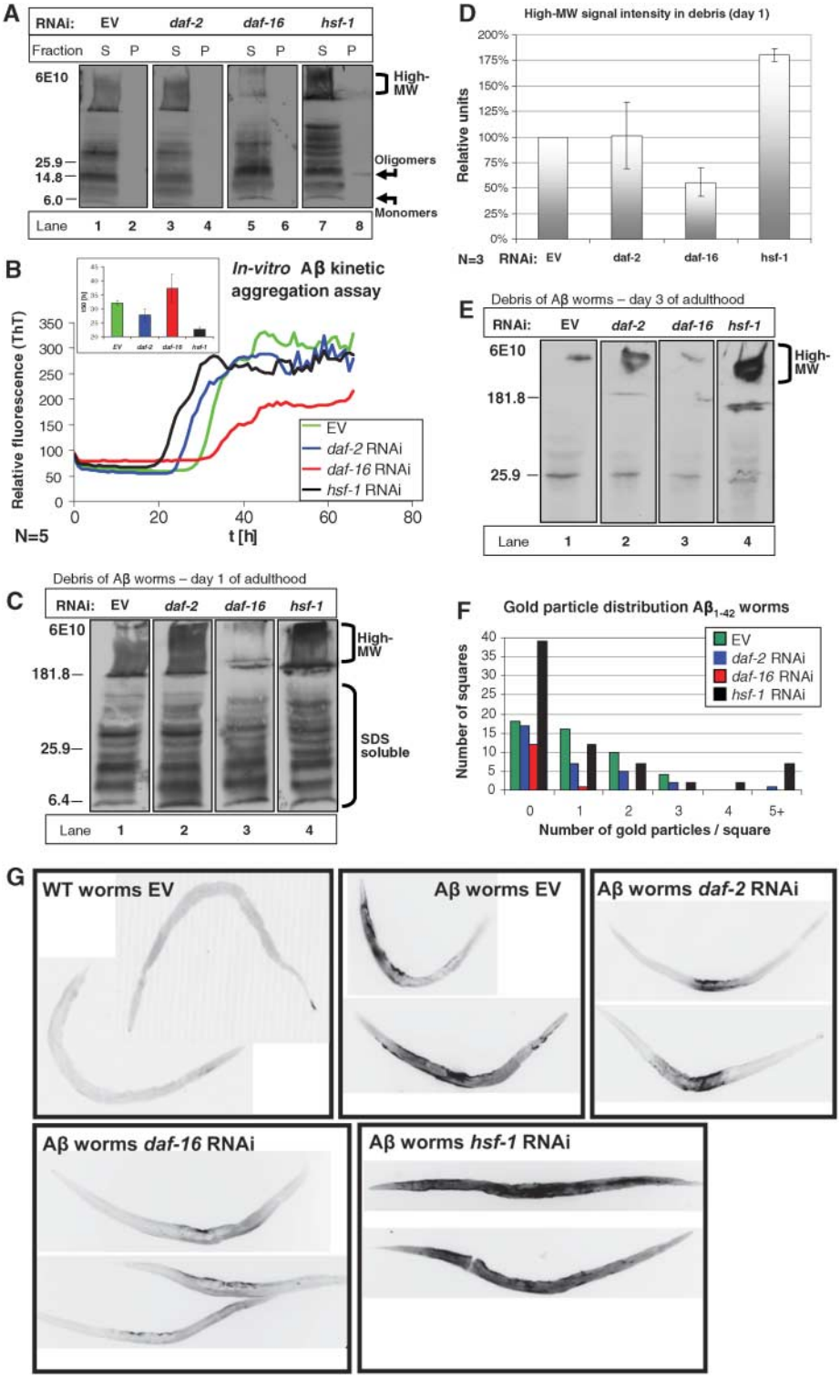


**Fig. 2.** Lack of correlation between $A\beta_{1-42}$ high-MW aggregates and toxicity. (**A**) $A\beta_{1-42}$ worms were fed bacteria expressing EV or double-stranded RNA of *daf-2*, *daf-16*, or *hsf-1* to day 1 of adulthood. The worms were homogenized, and equal amounts of PDS (fig. S5A) were incubated for 30 min on ice with 1% sarkosyl and spun for 1 hour in an ultracentrifuge (427,000 g). Supernatants and pellets were separated and loaded onto denaturing 12% polyacrylamide (PAA) gels and analyzed by WB using 6E10 monoclonal antibody (mAb). No Aβ signal was detected in pellets of EV, *daf-2*, and *daf-16* RNAi worm PDS (lanes 2, 4, and 6, respectively). A weak 16-kD Aβ band was detected in the pellet of PDS from *hsf-1* RNAi worms (lane 8, oligomers). (**B**) RNAi of $A\beta_{1-42}$ worms as in (A). PDS samples were prepared at day 1 of adulthood and were used to seed in vitro kinetic $A\beta_{1-40}$ aggregation reactions that were monitored by using thioflavin-T (ThT) fluorescence. PDS of *hsf-1* RNAi-treated animals (black) exhibited the most significant acceleration of the reaction, indicating the most seeding competent aggregates. *daf-2* RNAi (blue) accelerated the reaction compared with the EV (green), whereas *daf-16* RNAi (red) had the least seeding competent aggregates. (Inset) Statistical analysis of results obtained in (B). Error bars indicate standard deviations, $n = 5$. (**C**) $A\beta_{1-42}$ worms were grown and treated as in (A). Debris was analyzed by using 12% SDS PAA gel and WB. The largest amount of $A\beta_{1-42}$ high-MW aggregates was detected in animals with reduced *hsf-1* (lane 4); *daf-16* RNAi resulted in the least (lane 3), whereas *daf-2* RNAi (lane 2) had slightly more $A\beta_{1-42}$ high-MW aggregates. (**D**) Statistical analysis of the WB high-MW aggregate intensities in (C). Error bars indicate standard deviations, $n = 3$. (**E**) RNAi of $A\beta_{1-42}$ worms as in (A). Aβ contents of the worm debris were analyzed at day 3 of adulthood by using WB of a denaturing 4% PAA gel. The largest amount of high-MW $A\beta_{1-42}$ was detected in *hsf-1* RNAi worms (lane 4), followed by *daf-2* RNAi animals (lane 2); the least amount of $A\beta_{1-42}$ high-MW aggregates was found in *daf-16* RNAi animals (lane 3). (**F**) Quantification and distribution histogram analysis of gold particle labeling of the $A\beta_{1-42}$ worm preparations from immuno-EM analysis. EM images (fig. S10) were overlaid with a grid of 100 nm by 100 nm squares (Materials and Methods). Shown are distribution analyses of the number of immunogold particles found within squares that contained aggregate surfaces. The $A\beta_{1-42}$ immunogold staining signal of *hsf-1* RNAi worms is the most intense, whereas signal of $A\beta_{1-42}$ in *daf-16* RNAi treated worms is the weakest. (**G**) $A\beta_{1-42}$ worms were grown on RNAi bacteria as in (A) to day 2 of adulthood and were subjected to IF microscopy using the Aβ mAb 4G8. The signal intensity of *daf-2* RNAi worms was similar to that of EV worms. *daf-16* RNAi animals had the weakest signal, and *hsf-1* RNAi animals showed considerably stronger signal intensity. Wild-type animals not expressing $A\beta_{1-42}$ did not exhibit IF signal, demonstrating the specificity of the $A\beta_{1-42}$ mAb.

fibrils? Viability of rat adrenal pheochromocytoma (PC12) cells was discerned by the MTT assay (*24*) and normalized to cell survival when incubated in the absence of $A\beta_{1\text{-}40}$. Worm PDS dramatically reduced cytotoxicity of $A\beta_{1\text{-}40}$ aggregates prepared in vitro (Fig. 3E). Analogous results were obtained when resazurin (*25*) was used to measure $A\beta_{1\text{-}40}$ fibril toxicity on PC12 cells (fig. S12). Thus, disaggregation directly correlates with detoxification of $A\beta_{1\text{-}40}$ fibrils in these widely used cell-based assays.

Although HSF-1–regulated disaggregation activity could increase toxicity by releasing small toxic aggregates from larger less-toxic aggregates, our data point to the protective activity of HSF-1, suggesting a tight mechanistic link between disaggregation and degradation, possibly mediated by proteases such as the insulin-degrading enzyme (*26*) or neprilysin (*27*).

We measured the disaggregation activity of PDS from $A\beta_{1\text{-}42}$ worms grown on either EV, *daf-2*, *daf-16*, or *hsf-1* RNAi bacteria (Fig. 3F). Disaggregation curves were fit to an exponential decay function to quantify the results and to assess their statistical significance. No significant difference was observed among PDS of EV, *daf-2*, and *daf-16* RNAi worms. However, PDS of *hsf-1* RNAi worms exhibited a decreased disaggregation rate (35%, $N = 3$, $P < 0.03$), indicating that HSF-1 regulates the disaggregation activity (Fig. 3F inset). Nevertheless, the relatively small effect of *hsf-1* RNAi on disaggregation is unexpected given its robust physiological response on $A\beta_{1\text{-}42}$ toxicity. One possibility is that HSF-1 also regulates protective functions other than disaggregation. Alternatively, HSF-1 may be one component in a more complex mechanism that regulates disaggregation. It is also possible that the 35% decline in disaggregation results in exacerbated $A\beta_{1\text{-}42}$ proteotoxicity. In any case, reduced *hsf-1* slowed disaggregation whereas reduced *daf-16* did not, supporting the notion that HSF-1 regulates disaggregation.

**Small $A\beta_{1\text{-}42}$ oligomers correlate with toxicity.** The lack of correlation between proteotoxicity and large-MW aggregates suggests that small oligomers may be the key toxic species in the worm $A\beta_{1\text{-}42}$ aggregation model. Numerous lines of evidence implicate $A\beta_{1\text{-}42}$ oligomers in proteotoxicity (*28*–*30*). To determine whether small $A\beta_{1\text{-}42}$ aggregates correlate with toxicity, we grew worms to adulthood on EV, *daf-2*, *daf-16*, or *hsf-1* RNAi bacteria; subjected the PDS fractions to ultracentrifugation; and analyzed the soluble supernatants and insoluble pellets by WB (Fig. 2A). No Aβ was detected in the insoluble pellets of EV, *daf-2*, and *daf-16* RNAi-treated worms. However, a weak Aβ immunoreactive band of about 16 kD was detected in the insoluble pellet of *hsf-1* RNAi worms (Fig. 2A). This band size is consistent with a SDS-stabilized $A\beta_{1\text{-}42}$ trimer, possibly derived from a larger quaternary structure. When PDS incubation with 1% sarkosyl was shortened to 10 min, the 16-kD protein was

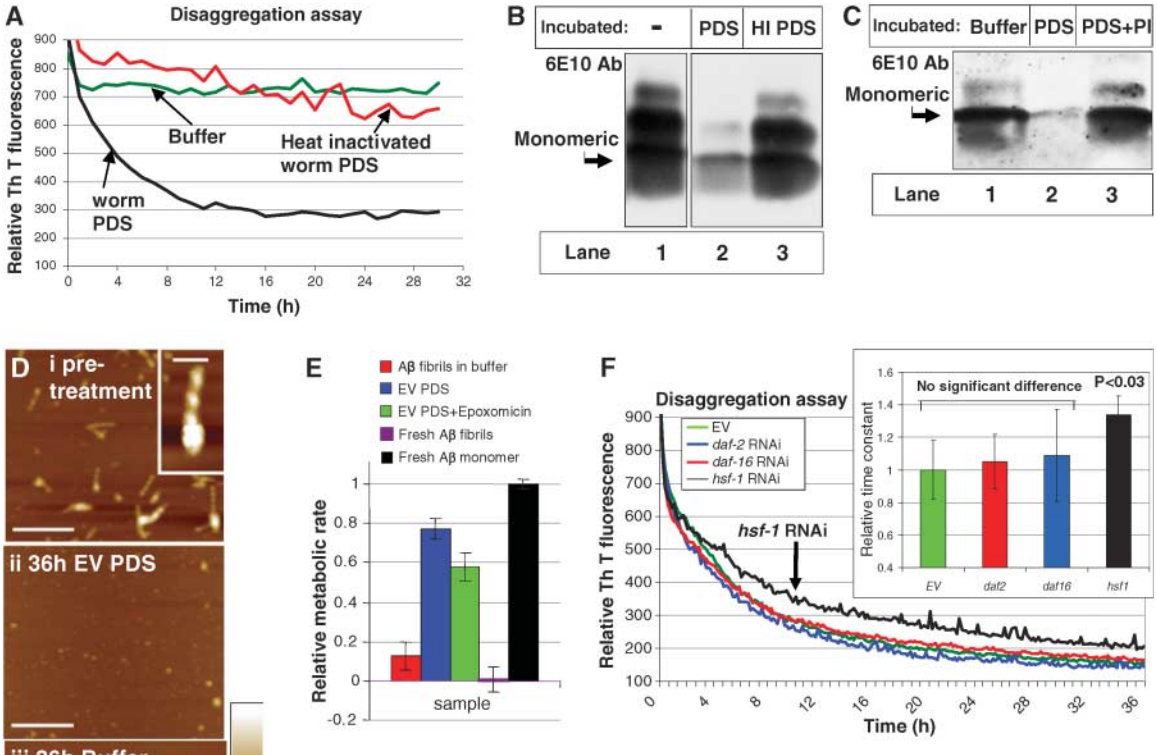


**Fig. 3.** *hsf-1* is required for efficient disaggregation of $A\beta_{1\text{-}42}$ aggregates. (**A**) Pre-aggregated, ThT-labeled $A\beta_{1\text{-}40}$ fibrils were incubated with either buffer (green), $A\beta_{1\text{-}42}$ worm PDS (black), or heat-inactivated PDS (red) in the presence of epoxomicin (10 μM). ThT fluorescence emission declined in the presence of worm PDS, indicating disaggregation activity. The $A\beta_{1\text{-}40}$ fibrils were stable in both buffer and heat-inactivated (HI) PDS. (**B**) Pre- and postdisaggregation samples were loaded onto 10% PAA gel. $A\beta_{1\text{-}40}$ was visualized by WB using 6E10 before the reaction (lane 1) and after 96 hours in the presence of worm PDS (lane 2) or in the presence of heat-inactivated PDS (lane 3). Less $A\beta_{1\text{-}40}$ was observed after incubation with worm PDS but not after incubation with heat-inactivated PDS. No proteasome inhibitors were used in this experiment. (**C**) Disaggregation reaction was performed in the absence and the presence of a protease inhibitor cocktail (PI) (lanes 2 and 3, respectively). WB analysis indicated that in the presence of PI, the total quantity of $A\beta_{1\text{-}40}$ did not change compared to the buffer-incubated fibrils, despite the disaggregation. (**D**) In vitro aggregated $A\beta_{1\text{-}40}$ fibrils were visualized by using AFM with no treatment (i), after a 36-hour incubation with EV-grown $A\beta_{1\text{-}42}$ worm PDS (ii), and after a 36-hour incubation with buffer only (iii). No large fibrils were detected after incubation with worm PDS. All large horizontal bars represent 1 μm; inset bar, 200 nm; and height scale bar, 20 nm. (**E**) Worm disaggregation activity reduces the $A\beta_{1\text{-}40}$ fibril-mediated cytotoxicity in cell-based assays. By using the disaggregation assay and conditions as in (B) and 72-hour incubation, we added $A\beta_{1\text{-}40}$ disaggregation samples (500 nM) to PC12 cell culture medium for 3 days. Cell viability was assayed by MTT metabolic activity (*24*). $A\beta_{1\text{-}40}$ toxicity was reduced in samples incubated with worm PDS in the presence (green) or absence (blue) of epoxomicin (10 μM). Samples incubated without worm PDS (red) showed similar toxicity to the starting material (purple). Monomeric $A\beta_{1\text{-}40}$ peptide did not exhibit toxicity under the assay conditions (black). Similar results were found with the use of a resazurin-based assay (fig. S12). (**F**) *hsf-1* is required for efficient disaggregation of pre-formed $A\beta_{1\text{-}40}$ fibrils. RNAi of $A\beta_{1\text{-}42}$ worms as in Fig. 2A. PDS of *hsf-1* RNAi worms (black) exhibited 20 to 50% decline in disaggregation activity compared with PDS of EV worms (green). There was no significant change in disaggregation activities in PDS of *daf-2* (blue) or *daf-16* (red) RNAi worms. (Inset) Statistical analysis of disaggregation results shown in (F) indicate that EV and *hsf-1* RNAi worms are significantly ($P < 0.03$) different ($n = 3$).

detected in all insoluble pellets (Fig. 4A). Notably, the amounts of the 16-kD species correlated with $A\beta_{1-42}$ toxicity; insoluble pellets from *daf-2* RNAi worms had the least intense signal, whereas *daf-16*, *hsf-1*, and EV RNAi worms had greater signal intensities. $A\beta_{1-42}$ monomers were detected in the supernatants of EV and *daf-2* RNAi worms but not in *daf-16* and *hsf-1* RNAi worms (Fig. 4A), suggesting that $A\beta_{1-42}$ monomers had formed trimers and/or larger assemblies thereof. In the absence of detergents, all of the $A\beta_{1-42}$ was retained in the insoluble pellet, suggesting that it may be associated with membranes. These observations are consistent with an $A\beta_{1-42}$ quaternary structure; apparently a trimer (16 kD) or an oligomer thereof mediating proteotoxicity, possibly in association with a membrane.

By using high resolution IF microscopy (Fig. 4B), we detected $A\beta_{1-42}$ aggregates along muscle fibers of $A\beta_{1-42}$ worms grown on either *hsf-1* or *daf-16* RNAi bacteria. Only a small amount of $A\beta_{1-42}$ aggregates was detected along muscular fibers of $A\beta_{1-42}$ worms grown on EV, and no such signal was detected in *daf-2* RNAi worms. These results support the hypothesis that small $A\beta_{1-42}$ oligomers in spatial proximity to the muscle fibers correlate with toxicity in this worm model and are consistent with recent studies showing that Aβ oligomers, potentially trimers, posses the highest toxicity toward hippocampal long-term potentiation of neural cells (*31*) and that Aβ trimer assemblies are involved in memory impairment of transgenic AD model mice (*32*).

**Model of DAF-16– and HSF-1–mediated protection against $A\beta_{1-42}$ aggregate proteotoxicity.** Our data suggests the following model for how *daf-2*–regulated pathways reduce aggregate mediated proteotoxicity (Fig. 5). First (stage 5-I), aggregation-prone peptides (such as $A\beta_{1-42}$) form small toxic aggregates constitutively. We suggest that cells have developed two mechanisms to detoxify these toxic misassemblies. The preferred detoxification route is to efficiently disaggregate the toxic oligomer and degrade the amyloidogenic peptide (stages 5-II and 5-V), a pathway that is positively regulated by HSF-1 (stage 5-A), perhaps via a subset of molecular chaperones (*33*). When this pathway is overtaxed, another activity transforms toxic low-MW oligomers into high-MW aggregates of lower toxicity. This mechanism (stage 5-III) is positively regulated by DAF-16 (stage 5-B) through its target genes. The cell ultimately has to get rid of these large aggregates by either degrading them using the HSF-1–controlled disaggregation and degradation machinery (stages 5-IV and 5-V) or possibly by their secretion (stage 5-VI). The opposing disaggregation (HSF-1) and aggregation (DAF-16) detoxification pathways both are negatively regulated by IIS signaling (stages 5-C and 5-D).

How does this model explain our results? (i) When *hsf-1* is reduced, disaggregation in stages 5-II and 5-IV is impaired. This leads to a reduction of disaggregation of small toxic aggregates and leaves the cell no alternative but to actively form less-toxic high-MW aggregates by using the DAF-16 regulated ma-

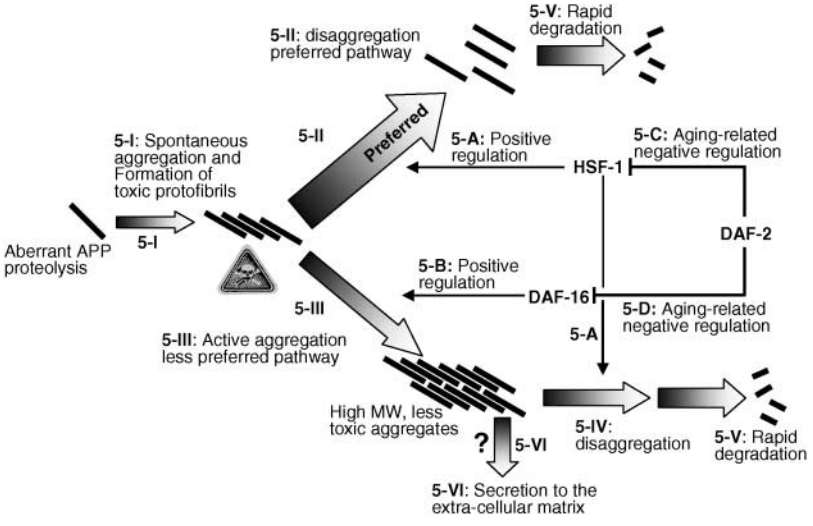


**Fig. 5.** Model of age-regulated HSF-1 and DAF-16 opposing anti-proteotoxicity activities. Aggregation-prone peptides spontaneously form small toxic aggregates (stage 5-I). Specialized cellular machinery identifies toxic aggregates and rapidly disaggregates and prepares them for degradation (stage 5-II). The products of this machinery are rapidly degraded (stage 5-V). This preferred mechanism is positively regulated by HSF-1 (stage 5-A) and negatively regulated by DAF-2 (stage 5-C). (Stage 5-III) When the HSF-1–regulated disaggregation machinery is overloaded, a secondary machinery that mediates aggregation is activated (stage 5-III), forming less-toxic high-MW aggregates. This machinery is positively regulated by DAF-16 (stage 5-B) and negatively by DAF-2 (stage 5-D). The high-MW aggregates, which accumulate as a result of the DAF-16–regulated mechanism, undergo either slow disaggregation and degradation by the HSF-1–regulated mechanism (stages 5-IV and 5V) or possibly secretion to the extracellular matrix (5-VI).

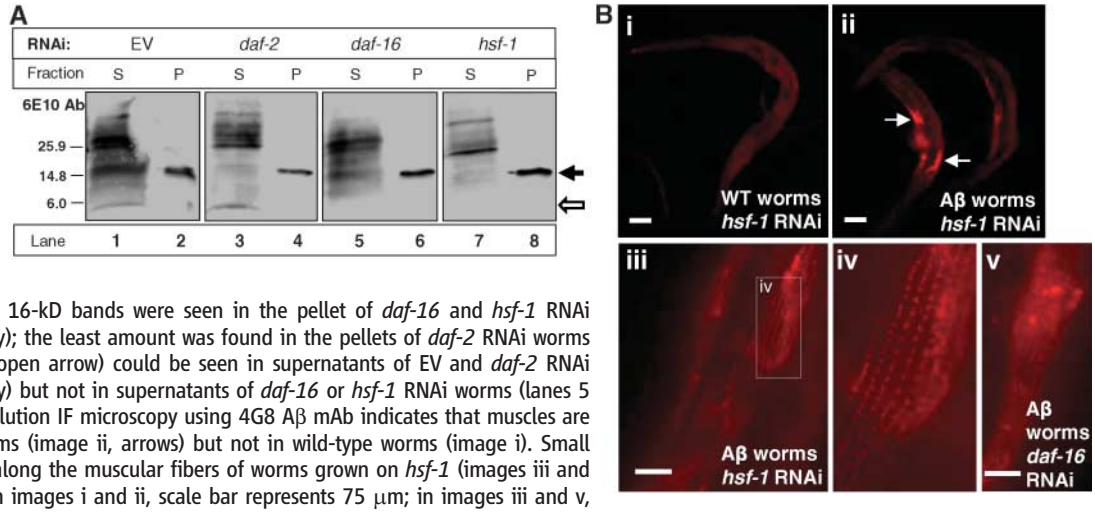


**Fig. 4.** Intensity of an Aβ immunoreactive 16-kD band correlates with toxicity. (**A**) Worm PDS supernatants and pellets were prepared as in Fig. 2A, except the PDS was incubated for 10 min on ice in 1% sarkosyl to maintain more proteins in their membrane-associated state. 16-kD Aβ bands were detected in all pellets (lanes 2, 4, 6 and 8, solid arrow). The most intense 16-kD bands were seen in the pellet of *daf-16* and *hsf-1* RNAi worms (lanes 6 and 8, respectively); the least amount was found in the pellets of *daf-2* RNAi worms (lane 4). Aβ monomers (~5-kD, open arrow) could be seen in supernatants of EV and *daf-2* RNAi worms (lanes 1 and 3, respectively) but not in supernatants of *daf-16* or *hsf-1* RNAi worms (lanes 5 and 7, respectively). (**B**) High resolution IF microscopy using 4G8 Aβ mAb indicates that muscles are labeled in *hsf-1* RNAi $A\beta_{1-42}$ worms (image ii, arrows) but not in wild-type worms (image i). Small $A\beta_{1-42}$ aggregates were detected along the muscular fibers of worms grown on *hsf-1* (images iii and iv) and *daf-16* RNAi (image v). (In images i and ii, scale bar represents 75 μm; in images iii and v, bar represents 15 μm).

chinery (stage 5-III). Moreover, the absence of HSF-1 also appears to slow the clearance of high-MW aggregates (stage 5-IV). Together, these activities lead to maximal accumulation of high-MW aggregates. (ii) When DAF-16 is reduced, cells lack the protective large-aggregate formation machinery, resulting in higher toxicity. Yet, the cells can disaggregate and degrade small aggregates (stage 5-II), resulting in fewer high-MW aggregates. The secondary importance of the DAF-16–regulated machinery explains why the toxicity of *daf-16* RNAi is lower than that of *hsf-1* RNAi. (iii) Inhibition of *daf-2*, a negative regulator of DAF-16 (stage 5-D) and perhaps of HSF-1 (stage 5-C) results in the up-regulation of both protective mechanisms: stages 5-II and 5-III. In this situation, both the clearance rate of small toxic aggregates and their detoxification by active aggregation are maximal, resulting in minimal toxicity. According to our model, the aging process actively reduces the cellular ability to detoxify small toxic aggregates by negative regulation of both detoxification mechanisms via the IIS pathway.

The IIS pathway plays a role in modulating other forms of toxic protein aggregation, such as in the aggregation of the huntingtin protein (*13*, *15*, *16*), suggesting that the activities identified here may be quite general. Additionally, small perturbations of proper protein-folding homeostasis have been demonstrated to have a profound impact on organismal integrity (*34*), suggesting that the protective mechanisms regulated by the IIS pathway may link longevity to protein homeostasis.

**References and Notes**


1. D. J. Selkoe, *Nature* **426**, 900 (2003).
2. R. R. Kopito, D. Ron, *Nat. Cell Biol.* **2**, E207 (2000).
3. E. Bossy-Wetzel, R. Schwarzenbacher, S. A. Lipton, *Nat. Med.* **10** (suppl.), S2 (2004).
4. B. Caughey, P. T. Lansbury, *Annu. Rev. Neurosci.* **26**, 267 (2003).
5. R. H. Takahashi *et al.*, *Am. J. Pathol.* **161**, 1869 (2002).
6. C. Kenyon, *Cell* **120**, 449 (2005).
7. K. D. Kimura, H. A. Tissenbaum, Y. Liu, G. Ruvkun, *Science* **277**, 942 (1997).
8. K. Lin, J. B. Dorman, A. Rodan, C. Kenyon, *Science* **278**, 1319 (1997).
9. S. Ogg *et al.*, *Nature* **389**, 994 (1997).
10. K. Lin, H. Hsin, N. Libina, C. Kenyon, *Nat. Genet.* **28**, 139 (2001).
11. C. Kenyon, J. Chang, E. Gensch, A. Rudner, R. Tabtiang, *Nature* **366**, 461 (1993).
12. M. Holzenberger *et al.*, *Nature* **421**, 182 (2003).
13. A.-L. Hsu, C. T. Murphy, C. Kenyon, *Science* **300**, 1142 (2003).
14. J. F. Morley, R. I. Morimoto, *Mol. Biol. Cell* **15**, 657 (2004).
15. J. F. Morley, H. R. Brignull, J. J. Weyers, R. I. Morimoto, *Proc. Natl. Acad. Sci. U.S.A.* **99**, 10417 (2002).
16. J. A. Parker *et al.*, *Nat. Genet.* **37**, 349 (2005).
17. C. D. Link *et al.*, *Neurobiol. Aging* **22**, 217 (2001).
18. C. Link, *Proc. Natl. Acad. Sci. U.S.A.* **92**, 9368 (1995).
19. A. Dillin, D. K. Crawford, C. Kenyon, *Science* **298**, 830 (2002).
20. C. A. Ross, M. A. Poirier, *Nat. Rev. Mol. Cell Biol.* **6**, 891 (2005).
21. K. Hasegawa, I. Yamaguchi, S. Omata, F. Gejyo, H. Naiki, *Biochemistry* **38**, 15514 (1999).
22. M. Arrasate, S. Mitra, E. S. Schweitzer, M. R. Segal, S. Finkbeiner, *Nature* **431**, 805 (2004).
23. F. Saudou, S. Finkbeiner, D. Devys, M. E. Greenberg, *Cell* **95**, 55 (1998).
24. M. Bucciantini *et al.*, *Nature* **416**, 507 (2002).
25. J. O'Brien, I. Wilson, T. Orton, F. Pognan, *Eur. J. Biochem.* **267**, 5421 (2000).
26. M. A. Leissring *et al.*, *Neuron* **40**, 1087 (2003).
27. N. Iwata *et al.*, *Science* **292**, 1550 (2001).
28. Y. Gong *et al.*, *Proc. Natl. Acad. Sci. U.S.A.* **100**, 10417 (2003).
29. D. M. Hartley *et al.*, *J. Neurosci.* **19**, 8876 (1999).
30. D. M. Walsh *et al.*, *Nature* **416**, 535 (2002).
31. M. Townsend, G. M. Shankar, T. Mehta, D. M. Walsh, D. J. Selkoe, *J. Physiol.* (2006).
32. S. Lesne *et al.*, *Nature* **440**, 352 (2006).
33. P. J. Muchowski, J. L. Wacker, *Nat. Rev. Neurosci.* **6**, 11 (2005).
34. T. Gidalevitz, A. Ben-Zvi, K. H. Ho, H. R. Brignull, R. I. Morimoto, *Science* **311**, 1471 (2006); published online 8 February 2006 (10.1126/science.1124514).


35. This study was generously supported by grants provided by the Backus and Ellison Medical Foundations (A.D.), NIH (DK 46335 and NS 50636), the Skaggs Institute of Chemical Biology, the Bundy Foundation, the Lita Annenberg Hazen Foundation, and the Max Planck Society (J.W.K. and J.B.). E.C. is supported by the John Douglas French Alzheimer's Foundation. We gratefully acknowledge M. Wood and the Microscopy Core Facility at the Scripps Research Institute for the preparation of immuno-EM samples and pictures, M. R. Ghadiri for use of AFM, G. Herradon for the gift of PC12 cells, the Caenorhabditis Genetics Center for CL2006 worms, and Dillin and Kelly lab members and D. Selkoe for critical comments during the course of this work.


**Supporting Online Material**

www.sciencemag.org/cgi/content/full/1124646/DC1
Materials and Methods
Figs. S1 to S12
References
Movies S1 and S2


5 January 2006; accepted 24 July 2006
Published online 10 August 2006;
10.1126/science.1124646
Include this information when citing this paper.


# Oldest Writing in the New World


**Ma. del Carmen Rodríguez Martínez,[1] Ponciano Ortíz Ceballos,[2] Michael D. Coe,[3] Richard A. Diehl,[4] Stephen D. Houston,[5]* Karl A. Taube,[6] Alfredo Delgado Calderón[1]**



A block with a hitherto unknown system of writing has been found in the Olmec heartland of Veracruz, Mexico. Stylistic and other dating of the block places it in the early first millennium before the common era, the oldest writing in the New World, with features that firmly assign this pivotal development to the Olmec civilization of Mesoamerica.


Several writing systems are known from pre-Columbian Mesoamerica, most with dates after the first millennium before the common era (BCE). (*1*). Previously, no script has been associated unambiguously with the Olmec civilization, in many respects the progenitor of all later complex societies of Mexico and adjacent Central America (*2*). Recent proposals for late Olmec writing at La Venta, Tabasco, Mexico, rest on two categories of object, roller-seal iconography and isolated, discontinuous incisions, neither sure to be script (*3*). We report here on an Olmec

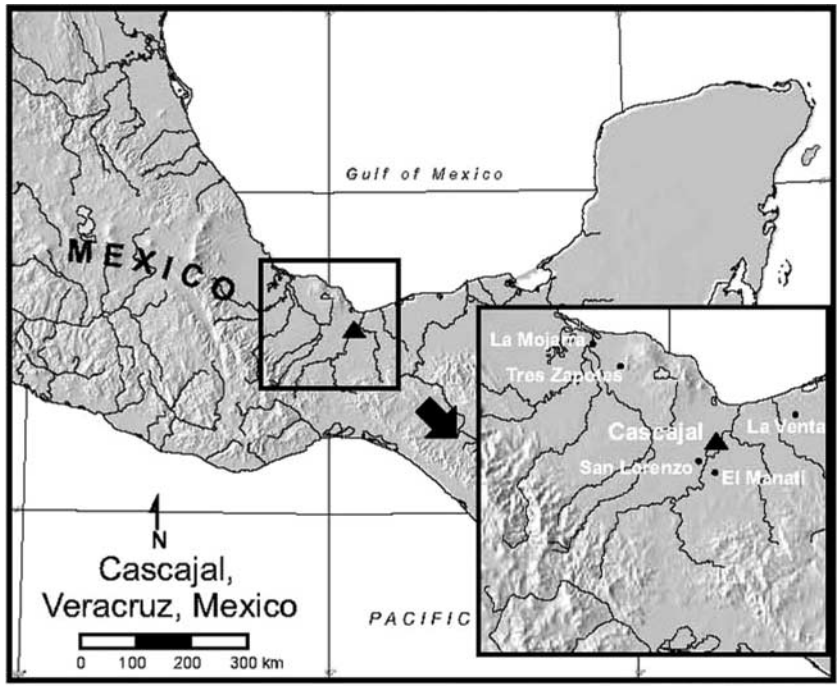


**Fig. 1.** Map showing location of Cascajal, Veracruz. Figure was prepared by Z. Nelson, Geography Department, Brigham Young University.